NJC

PAPER

View Article Online
View Journal | View Issue

TiO_2@C composite nanospheres with an optimized homogeneous structure for lithium-ion batteries

Cite this: *New J. Chem.*, 2014, **38**, 3722

Jun Zhang,*[ab] Jiangfeng Ni,[c] Jing Guo[a] and Bingqiang Cao*[a]

Received (in Montpellier, France) 22nd February 2014,
Accepted 20th May 2014

DOI: 10.1039/c4nj00263f

www.rsc.org/njc

Homogeneous TiO_2@C composite nanospheres are synthesized by a direct pyrolysis strategy using Ti-containing organic–inorganic polymers as precursors. The TiO_2@C composite nanospheres possess uniform distribution of tiny TiO_2 nanoparticles confined in the carbon matrix with a homogeneous structure. The carbon phase can not only improve the conductivity but also prevent the aggregation of TiO_2 nanoparticles. When evaluated as anodes for lithium-ion batteries, the TiO_2@C nanocomposites demonstrate a high reversible specific capacity of 207 mA h g^{-1} at 0.5 C (1 C = 250 mA g^{-1}) after 50 cycles and a stable cycling performance in comparison to pure TiO_2 nanospheres. This work offers a new pathway for realization of carbon-based composite materials for use as high performance anodes in LIBs.

Introduction

Lithium-ion batteries (LIBs) have been considered to be some of the most promising energy storage and conversion technologies to fulfil the ever-growing demand in both small consumer electronic devices and large-scale applications, such as electric vehicles (EV), hybrid electric vehicles (HEV), and stationary energy storage.[1,2] Practical applications of LIBs critically relied on the electrode materials with high capacity, high rate capability, good stability and safety. The current widely used anode in LIBs is graphite. In spite of its excellent electrical conductivity, the graphite anode suffers from a low Li-ion diffusion coefficient and the risk of formation of lithium dendrites, which might cause serious safety problems.[3]

TiO_2, as one of the most investigated semiconductor metal oxides, has attracted considerable attention for application in many fields, such as solar cells, photocatalysis, gas sensors, and LIBs.[4–8] For use as an anode for LIBs, TiO_2 features a series of merits including the low cost, low toxicity, high capacity, high current rate performance, and improved electrochemical stability.[3] However, the poor electronic and Li-ion conductivities have significantly limited its potential application in LIBs. To alleviate such problems, many strategies have been developed to improve the performance of TiO_2 anodes. For example, the controllable fabrication of TiO_2-based nanomaterials with desired structures or morphologies has proved to be very effective to improve the performance of LIBs. Lou *et al.*[9,10] demonstrated that TiO_2 hollow nanostructures could deliver better properties in terms of higher capacity, better rate capability, and good cycling performance. TiO_2 nanosheets with engineered (001) crystal facets have manifested enhanced electrochemical performances due to the accelerated Li-ion diffusion kinetics in specific crystal direction and adequate electrode–electrolyte contact.[11,12] Decreasing the particle size from the micrometer to the nanometer scale is also key to improved Li-ion diffusion because of the reduced diffusion length.[2,13] Ren *et al.* have shown that TiO_2 nanoparticles with the ever smallest size (<4.3 nm) are superior in Li-ion and charge storage compared with other bulk, nanowires, and nanotube morphologies.[14]

While great progress has been obtained by the nanostructuring strategy, a well-established and more reliable approach is to fabricate composite electrode materials by coating or mixing a host material with guest additives such as conductive carbon.[15–18] A great improvement in the specific capacity, rate performance, and cycling stability can be expected, because the carbon additive could significantly improve the surface electronic conductivity and the electric contact between electrodes and the surrounding active agents.[15] Zhao *et al.* proposed incorporation of a 3D carbon mixed conducting network in electrode materials, which allows for both fast Li-ion and electron migration.[19] TiO_2@carbon composite nanofibers prepared by the combination of electrospinning and subsequent thermal treatments also exhibited excellent cycling stability and rate capability as anode materials.[20]

[a] *Key Laboratory of Inorganic Functional Materials in Universities of Shandong, School of Materials Science and Engineering, University of Jinan, Jinan 250022, China. E-mail: mse_zhangj@ujn.edu.cn, mse_caobq@ujn.edu.cn*
[b] *Key Laboratory of Advanced Energy Materials Chemistry (Ministry of Education), Collaborative Innovation Center of Chemical Science and Engineering (Tianjin), College of Chemistry, Nankai University, Tianjin 300071, China*
[c] *School of Energy, Soochow University, Suzhou 215006, China*

Park *et al.*[21,22] reported that carbon-coated TiO_2 nanotubes synthesized with very low carbon content could manifest high rate capability and power performance. Wang[23] and Guo[24] *et al.* reported mesoporous TiO_2–C composite anodes with excellent rate capability and cycling performance. Very recently, Petkovich[25] and Wang[26] *et al.* used a one-pot pyrolysis to produce 3DOM TiO_2–C and CNT@TiO_2–C composite materials for LIB anodes with high rate performance. To further optimize the electrochemical performance of TiO_2-based anodes with low cost, it is desirable to develop a simple procedure for synthesizing TiO_2@carbon composite anode materials, in which nanometer-sized TiO_2 particles are homogeneously dispersed in a conductive carbon matrix. Such an optimized structure would enable fast electron transport between nanoparticles, thus improving the electrochemical performance.

In this work, we propose a direct pyrolysis route at moderate temperature to prepare homogeneous TiO_2@C composite nanospheres by using Ti-containing colloidal organic–inorganic polymers as precursors. The new attempt using organic–inorganic polymer spheres as both carbon and TiO_2 sources has advantages of generation of a carbon phase closely coated on TiO_2 nanoparticles and suppression of the particle growth to yield homogeneous conductive nanocomposites. When evaluated as the anodes for LIBs, the TiO_2@C composite nanospheres manifest excellent charge–discharge properties with relatively high capacity, good rate capability, and stable cycling performance.

Experimental section

Synthesis of homogeneous TiO_2@C composite nanospheres

Organic–inorganic polymer nanospheres containing Ti were prepared according to the literature method with some modifications.[27,28] In a typical synthesis, 2 mL of tetrabutyl titanate (TBT) was added to 50 mL of ethylene glycol (EG) under magnetic stirring for 10 h, then the mixture was transferred into a solution containing 2.7 mL water and 170 mL acetone. After further stirring for 1 h, the white colloidal organic–inorganic polymers were harvested by centrifugation and washing with water and ethanol several times, and dried at 80 °C. The as-obtained organic–inorganic nanospheres are indeed titania glycolate polymers and have an amorphous structure.[27] Homogeneous TiO_2@C nanocomposites were readily obtained by pyrolysis of the organic–inorganic nanospheres in a N_2 atmosphere at 500 °C for 4 h. For comparison, pristine TiO_2 nanospheres were also synthesized by annealing the polymers in air at 500 °C for 4 h.

Characterization

The crystal phase and structure of samples were identified by power X-ray diffraction (XRD) using a Bruker diffractometer (D8-Advance) with Cu Kα radiation of 1.5418 Å. Thermogravimetric analysis (TG) was performed on a Mettler-Toledo TGA/DSC 1/1600HT at a heating rate of 5 °C min^{-1} in air. The size, morphology and composition of the samples were characterized by scanning electron microscopy (SEM, Quanta FEG 250, 30 kV), transmission electron microscopy (TEM, JEM-1011, 100 kV), high resolution transmission electron microscopy (HRTEM, JEOL-2010, 200 kV), energy dispersive X-ray spectroscopy (EDS, JEOL-2010, 200 kV), and N_2 adsorption–desorption analysis (JW-BK122W).

Electrochemical characterization

2032 coin-type cells were used for electrochemical tests. The composite electrode sheets consisting of 70 wt% active material, 20 wt% acetylene black, and 10 wt% polytetrafluoroethylene (PTFE) were used as cathodes. Lithium metal foil was used as counter and reference electrodes. The electrolyte solution is 1 M LiPF6 dissolved in a mixture of ethylene carbonate (EC) and dimethyl carbonate (DMC) in a volume ratio of 1 : 1. Galvanostatic tests were carried out using a Land battery test system at 28 °C (1 C was defined as 250 mA g^{-1}). Electrochemical impedance spectroscopy (EIS) tests were performed on a Zennium electrochemical workstation tester.

Results and discussion

Morphology and structure investigation

The Ti-containing organic–inorganic polymer nanospheres were prepared by an improved sol–gel method, by which the hydrolysis of TBT was controlled to occur slowly to obtain homogeneous nucleation and growth.[27] Fig. 1a shows that the polymer nanospheres have a sphere-like shape, and some spheres are seen to fuse together. The inset in Fig. 1a shows the size distribution histogram, which indicates that the nanospheres have a diameter in the range of 250–550 nm, with an average size of 377 nm. After calcination at a moderate temperature of 500 °C in N_2, the organic–inorganic polymers can be converted into TiO_2@C nanospheres. Fig. 1b displays the SEM image of the composite TiO_2@C nanospheres, revealing that the TiO_2@C nanospheres well preserve the spherical morphology after thermal annealing. Interestingly, the TiO_2@C nanospheres have a smaller size as compared with the polymer precursor in Fig. 1a. The reduced size and dimension of the composite nanospheres is probably caused by removal of water and decomposition of the organic component under the annealing process, resulting in the shrinkage of precursor spheres.

The thermal behavior of the precursor polymer and TiO_2@C spheres has been examined by TG analysis. In Fig. 2, the TG

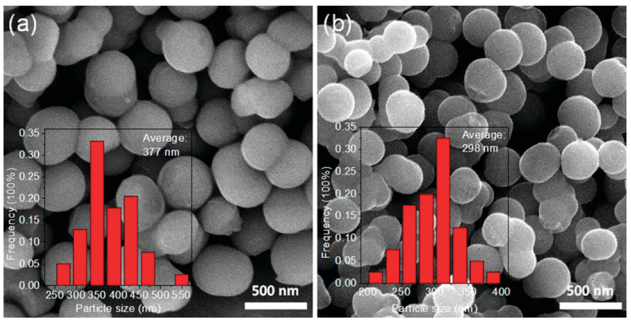

Fig. 1 SEM images of (a) Ti-containing organic–inorganic polymers and (b) TiO_2@C composite nanospheres obtained by pyrolysis of the Ti-containing polymers.

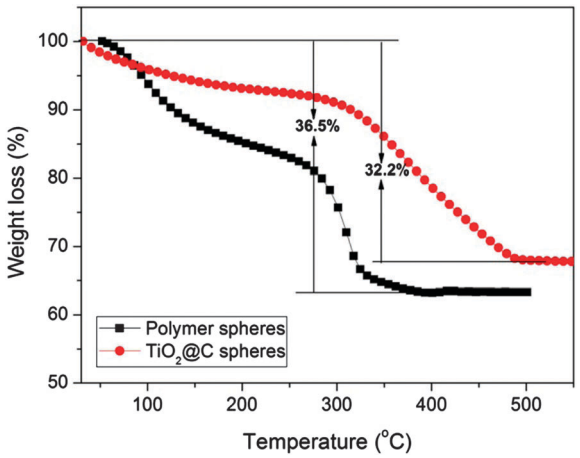

Fig. 2 TG analysis of Ti-containing organic–inorganic polymers and TiO_2@C nanospheres.

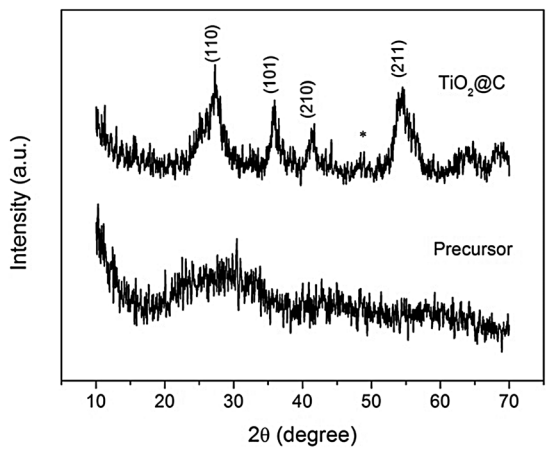

Fig. 3 XRD patterns of the polymer precursor and TiO_2@C nanospheres.

curve of the precursor polymer reveals a total weight loss of 36.5%, consisting of two steps of weight loss that can be ascribed to the evaporation of water molecules below 150 °C and the thermal decomposition or combustion of organic compounds such as ethylene glycol in the polymers between 150 and 400 °C. The curve of TiO_2@C spheres also shows two steps of weight loss of water evaporation and combustion of the thermally decomposed carbon phase. The carbon content in the TiO_2@C spheres is about 32.2%.

The crystalline phase of the polymer precursor and TiO_2@C nanospheres has been studied by XRD. Fig. 3 demonstrates that the polymer precursor has an amorphous structure, while the TiO_2@C sample shows a dominant structure of rutile TiO_2 (JCPDS No.65-0190) and a trace amount of anatase TiO_2 (JCPDS No. 21-1272) as indicated by an asterisk. The crystallite size of TiO_2@C is estimated to be 11.2 nm from the full width at half maximum (FWHM) of (211) diffraction peak by using the Scherer equation. After annealing under a N_2 atmosphere, the organic compounds in the precursor would be carbonized through pyrolysis and eventually transform into carbon.

The detailed structure and morphology of the samples have been further characterized by TEM. Fig. 4(a–d) exhibit the representative TEM images of TiO_2@C nanospheres with different magnifications. As can be seen in Fig. 4a and b, the TiO_2@C particles have a sphere-like morphology. A closer observation of the individual nanosphere in Fig. 4b reveals that the TiO_2@C nanosphere shows a homogenous structure. From Fig. 4c it is seen that the sphere contains many discrete nanoparticles confined in a carbon matrix with a small size of 8–18 nm. Under annealing in N_2, the organic molecules cannot burn off and subsequently converted into carbon through pyrolysis. During the carbonization process at 500 °C in N_2, TiO_2 nanoparticles are formed with better crystallization and simultaneously a carbon phase is formed around the TiO_2 nanoparticles, leading to the formation of a homogeneous nanocomposite of TiO_2@C with TiO_2 nanoparticles highly distributed in carbon. The inset of Fig. 4c

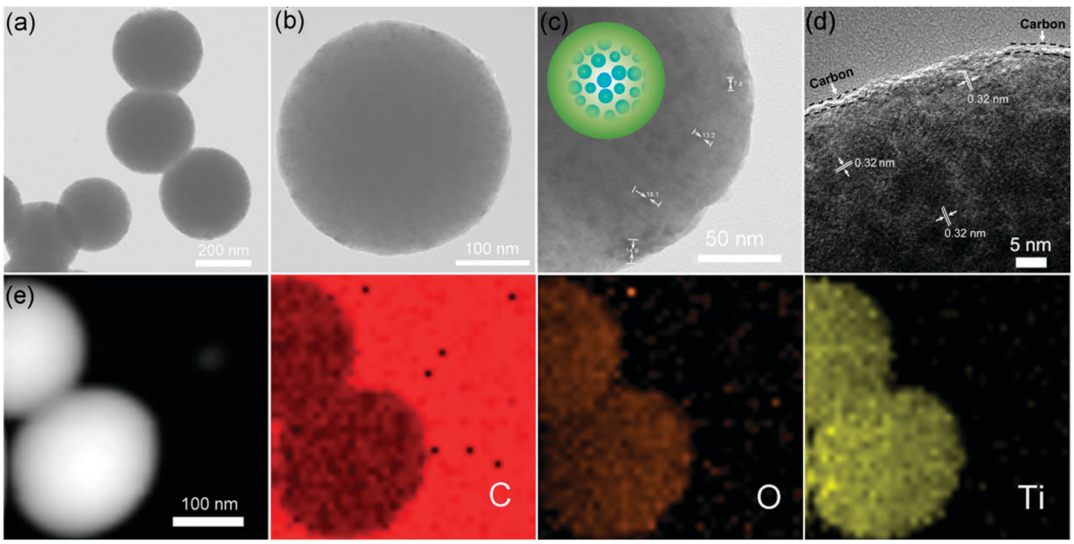

Fig. 4 (a–c) TEM, (d) HRTEM images and (e) element mapping of TiO_2@C nanospheres.

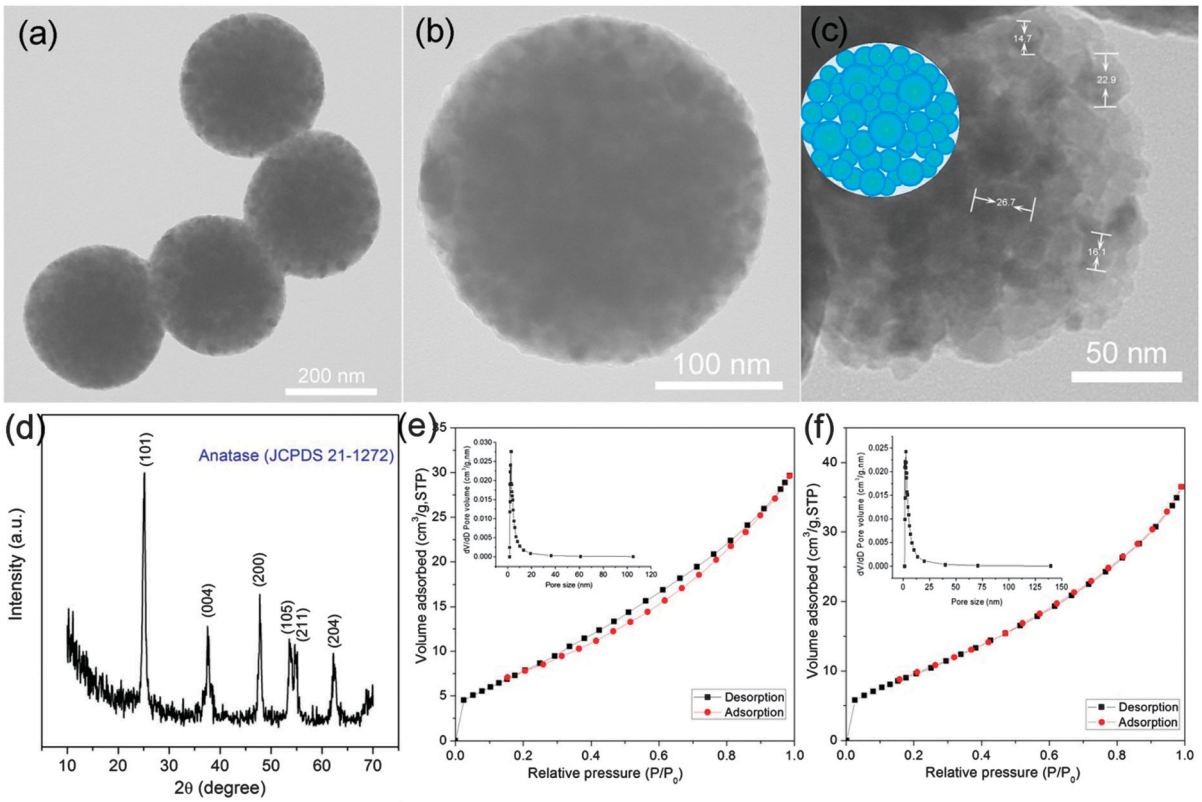

Fig. 5 (a–c) TEM images and (d) XRD pattern of pure TiO_2 nanospheres obtained by calcination of the Ti-containing polymers in air, and N_2 adsorption–desorption analysis of (e) TiO_2 and (f) TiO_2@C.

illustrates the homogeneous structure of the TiO_2@C composite nanospheres. Fig. 4d shows the HRTEM image of a TiO_2@C nanosphere. A carbon layer around the sphere edge can be seen clearly, as indicated by the arrows. The clear lattice fringes reveal the highly crystalline nature of the TiO_2 nanoparticles confined in carbon. The interplane spacing of 0.32 nm corresponds to the (110) planes of rutile TiO_2. The elemental composition of the sample was further studied by the local elemental mapping technique using EDS mounted on HRTEM. The results are shown in Fig. 4e. It is apparent that the particle has a uniform distribution of all the elements (C, O, and Ti), which further demonstrate the homogeneous structure of TiO_2@C composite nanospheres.

For comparison, pure TiO_2 nanospheres were also prepared by directly annealing the Ti-containing organic–inorganic polymer nanospheres in air. Fig. 5(a–c) exhibit the SEM images of pure TiO_2 nanospheres. As can be seen in Fig. 5a and b, the TiO_2 particles also possess a sphere-like morphology. A closer observation of the individual nanospheres in Fig. 4b and 5b, reveals that the former has a relatively rough surface. Nanoparticles with different diameters can be easily distinguished due to the image contrast. Fig. 5c indicates that the TiO_2 nanosphere is comprised of numerous aggregated nanoparticles with a size range of 14–27 nm. When calcined in air, the organic component in the polymer spheres could be completely removed and TiO_2 nanoparticles nucleated and grew together to constitute the spheres. The schematic illustration in the inset of Fig. 5c simulates the structure of pure TiO_2 nanospheres, which is assembled by many TiO_2 nanoparticles with different size. The XRD pattern in Fig. 5d suggests that the pure TiO_2 nanospheres have an anatase structure, with all the diffraction peaks being consistent with JCPDS 21-1272. The mean crystallite size estimated from the full width at half maximum (FWHM) of the (101) peak is *ca.* 17.7 nm, which is much larger than that (11.2 nm) of TiO_2@C composites. This indicates that the annealing atmosphere has a significant influence on the crystallite size of the products. Annealing in air is able to burn off the organic component and obtain pure inorganic TiO_2 nanospheres. If the annealing process is performed in N_2, the organic compounds will be carbonized through pyrolysis and eventually transform into carbon. It is deduced that the formed carbon phase around TiO_2 could effectively suppress the growth of TiO_2 nanoparticles. Recent studies by Petkovich[25] and Huang *et al.*[29] reported a similar result at temperatures of 800 and 1100 °C. The Brunauer–Emmett–Teller (BET) specific surface area and porous structure of TiO_2 and TiO_2@C have been obtained by N_2 adsorption–desorption analysis, which are shown in Fig. 5e and f. The BET surface area of TiO_2 is evaluated to be 36.8 $m^2\ g^{-1}$, which is a little larger than that (31.1 $m^2\ g^{-1}$) of the TiO_2@C composite. This is because pure TiO_2 nanospheres are an aggregation of TiO_2 nanoparticles with rich inner-particle space. Furthermore, the insets in Fig. 5e

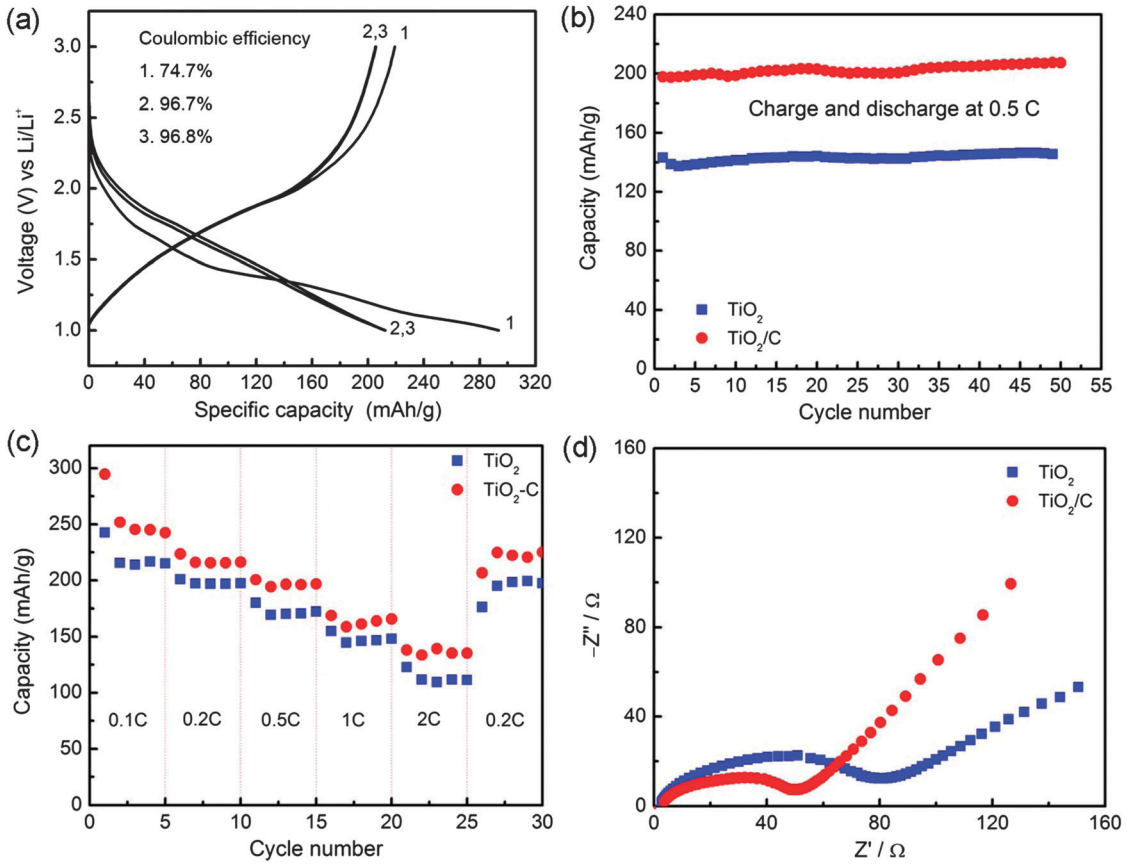

Fig. 6 (a) Discharge–charge voltage profiles at 0.2 C, (b) cycling performance at 0.5 C, (c) rate capability from 0.1 C to 2 C, and (d) Nyquist plots of TiO_2 and TiO_2@C nanospheres.

and f show the Barrett–Joyner–Halenda (BJH) pore size distribution, revealing that both samples have a mesoporous structure with pore size in the range of 2–50 nm.

Electrochemical performance

Such a TiO_2@C structure is very promising for use as a LIB anode material, as the carbon component can greatly enhance the electronic conductivity between the TiO_2 nanoparticles. In addition, the carbon matrix can also effectively prevent the aggregation of nanoparticles during cycling.[30]

We thus further evaluate the electrochemical performance of these unique homogeneous TiO_2@C nanospheres for LIBs. Fig. 6a shows the first three consecutive discharge–charge voltage profiles of the TiO_2@C composite nanospheres at a 0.2 C rate in the voltage range of 1.0–3.0 V. The initial discharge and charge capacities are found to be 293.6 and 219.3 mA h g^{-1}, respectively, indicating an initial coulombic efficiency of 74.7%. Such an initial discharge capacity is even higher than the theoretical capacity (233 mA h g^{-1}) of TiO_2@C nanospheres. The theoretical capacity of TiO_2@C nanospheres is calculated based on the weight content and theoretical capacities of TiO_2 (67.8 wt%, 168 mA h g^{-1}) and carbon (32.2 wt%, 372 mA h g^{-1}). The extra lithium storage capacity might be associated with the phenomenon of interface storage due to the unique composite structure and the carbon phase. While for the second and third cycles, the discharge and charge capacities are 212.2 and 205.4 mA h g^{-1} and 212.3 and 205.7 mA h g^{-1}, respectively, corresponding to a coulombic efficiency of 96.7% and 96.8%. Compared with the initial discharge capacity (293 mA h g^{-1}), the second discharge shows an irreversible capacity of 80 mA h g^{-1}. The capacity loss may be caused by the inserted Li-ions in the irreversible sites of TiO_2 nanoparticles[31,32] and other side reactions arising from the trace amount of water absorbed onto electrode materials[32] at the first stage of discharge–charge processes. A similar phenomenon has also been previously observed for various TiO_2 polymorphs, such as TiO_2(B),[12,33] anatase,[19,20] and rutile.[31,34]

The cycling performance of pure TiO_2 and TiO_2@C composite nanospheres has been tested at 0.5 C. As shown in Fig. 6b, although both TiO_2@C and TiO_2 exhibit good cycling stability, the TiO_2@C nanocomposite possesses apparently much higher capacity than pure TiO_2. The higher capacity of TiO_2@C might be due to the carbon phase, which has a higher theoretical capacity than TiO_2. After 50 cycles of discharge–charge at 0.5 C, the TiO_2@C nanospheres can still deliver a high reversible specific capacity of 207 mA h g^{-1}, which is much higher than that (145.6 mA h g^{-1}) of pure TiO_2 nanospheres and is also better than the reported results for TiO_2–C nanocomposite[20,24,35,36] and TiO_2 nanotubes[8] and nanoparticles[37] at a similar current density. In addition, the pure TiO_2 nanospheres have an anatase

structure, which is generally considered to be more electrochemically active than the rutile polymorph for Li-insertion.[38,39] The above results clearly demonstrate the superior lithium storage performance of the rutile TiO_2-based composite to anatase as an anode material.

The rate capability of the TiO_2@C nanospheres is also tested at different current densities. As shown in Fig. 6c, the TiO_2@C anode is observed to exhibit much higher reversible capacity and good cycling stability than TiO_2. The TiO_2@C nanocomposite presents very good cycling response to continuously varying current rates from 0.1 to 2 C. At various current densities, the TiO_2@C composite anode can retain discharge capacities of 242.6, 216.2, 197.1, 165.5 and 134.3 mA h g^{-1} after 5 cycles at current rates of 0.1, 0.2, 0.5, 1 and 2 C, respectively, while the pure TiO_2 nanospheres only deliver discharge capacities of 215.5, 196.7, 172.1, 147.3 and 110.6 mA h g^{-1}. Furthermore, when the discharge–charge test is re-cycled at 0.2 C after 2 C, the TiO_2@C nanocomposite can still deliver a discharge capacity of about 220 mA h g^{-1}. This value is almost identical to the former 0.2 C test, suggesting a high electrochemical stability of the homogenous TiO_2@C nanocomposites.

In order to understand the improved performance of TiO_2@C nanocomposites, the electrochemical impedance spectroscopy (EIS) tests for both TiO_2@C and pure TiO_2 have been performed. As displayed in Fig. 6d, the Nyquist plots of both TiO_2@C and pure TiO_2 consist of one semicircle in the high-frequency region and a bias line in the low-frequency region. The radius of the semicircle is correlated with the charge-transfer ability of the corresponding electrode. Apparently, the TiO_2@C electrode possesses a much lower resistance (50 Ω) than the pure TiO_2 electrode (81 Ω), as a result of good electrical contact between TiO_2 and carbon. This indicates that the TiO_2@C composite electrode possesses lower charge-transfer impedance due to the uniform carbon matrix around TiO_2 nanoparticles. Consequently, both the Li^+ diffusion and electron transfer are effectively expedited at high cycling rates for the TiO_2@C composite electrode, leading to superior capacity retentions at different current rates in comparison to pure TiO_2 nanospheres.

Based on the above discussion, the TiO_2@C nanocomposite has demonstrated much better performance than the pure TiO_2 anode. Several factors may account for the enhanced lithium storage properties. First, TiO_2@C has higher electronic conductivity for electron transfer due to uniform carbon coating.[20,24,30,35,40] Second, the small size of TiO_2 nanoparticles confined in carbon also provides a short path for lithium intercalation and de-intercalation.[14,31] Third, the optimized homogeneous TiO_2@C structure might also contribute to the improved performance, as it delivers a higher capacity during cycling when compared with other forms of the TiO_2–C nanocomposite,[24,35,36] possibly because the carbon matrix could effectively prevent the aggregation of TiO_2 nanoparticles.

Conclusions

In summary, a direct pyrolysis strategy has been proposed to realize an optimized structure of homogenous TiO_2@C nanocomposites by using Ti-containing organic–inorganic polymers as the precursors. The organic component can be easily converted to carbon, which can effectively suppress the growth of nucleated TiO_2 nanoparticles and simultaneously enable the TiO_2 nanoparticles to highly distribute in the carbon matrix. Electrochemical tests demonstrate that the as-synthesized TiO_2@C composite nanospheres exhibit an improved Li-ion storage performance in terms of higher capacity, better cycling performance and rate capability compared with pure TiO_2 nanospheres. The enhanced properties can be ascribed to the unique homogeneous structure of TiO_2@C, small size of TiO_2 nanoparticles, and improved conductivity due to the carbon matrix. It is expected that the proposed direct pyrolysis route in this work can also be utilized to fabricate other composite electrode materials for high performance lithium-ion batteries.

Acknowledgements

This work was supported by the Program for New Century Excellent Talents in University (NCET-11-1027) of MOE, China, the Taishan Scholar Professorship (TSHW20091007), the Open Project of Key Laboratory of Advanced Energy Materials Chemistry of Nankai University (KLAEMC-OP201201), and Shandong Provincial Science Foundation for Disguised Youth Scholars (JQ201214) and Excellent Young and Middle-aged Scientists (BS2012CL003).

Notes and references

1 B. Dunn, H. Kamath and J.-M. Tarascon, *Science*, 2011, **334**, 928–935.
2 P. G. Bruce, B. Scrosati and J. M. Tarascon, *Angew. Chem., Int. Ed.*, 2008, **47**, 2930–2946.
3 G.-N. Zhu, Y.-G. Wang and Y.-Y. Xia, *Energy Environ. Sci.*, 2012, **5**, 6652–6667.
4 J. Qu, Q. D. Wu, Y. R. Ren, Z. Su, C. Lai and J. N. Ding, *Chem. – Asian J.*, 2012, **7**, 2516–2518.
5 X. Chen and S. S. Mao, *Chem. Rev.*, 2007, **107**, 2891–2959.
6 J. F. Qian, M. Zhou, Y. L. Cao, X. P. Ai and H. X. Yang, *J. Phys. Chem. C*, 2010, **114**, 3477–3482.
7 A. S. Aricò, P. Bruce, B. Scrosati, J.-M. Tarascon and W. Van Schalkwijk, *Nat. Mater.*, 2005, **4**, 366–377.
8 A. Lamberti, N. Garino, A. Sacco, S. Bianco, D. Manfredi and C. Gerbaldi, *Electrochim. Acta*, 2013, **102**, 233–239.
9 Z. Wang and X. W. D. Lou, *Adv. Mater.*, 2012, **24**, 4124–4129.
10 S. J. Ding, J. S. Chen, Z. Y. Wang, Y. L. Cheah, S. Madhavi, X. A. Hu and X. W. Lou, *J. Mater. Chem.*, 2011, **21**, 1677–1680.
11 J. S. Chen, Y. L. Tan, C. M. Li, Y. L. Cheah, D. Luan, S. Madhavi, F. Y. C. Boey, L. A. Archer and X. W. Lou, *J. Am. Chem. Soc.*, 2010, **132**, 6124–6130.
12 S. Liu, H. Jia, L. Han, J. Wang, P. Gao, D. Xu, J. Yang and S. Che, *Adv. Mater.*, 2012, **24**, 3201–3204.
13 M. Wagemaker and F. M. Mulder, *Acc. Chem. Res.*, 2013, **46**, 1206–1215.
14 Y. Ren, Z. Liu, F. Pourpoint, A. R. Armstrong, C. P. Grey and P. G. Bruce, *Angew. Chem.*, 2012, **124**, 2206–2209.

15 H. Li and H. Zhou, *Chem. Commun.*, 2012, **48**, 1201–1217.
16 C. Wang, H. Li, A. Fu, J. Liu, W. Ye, P. Guo, G. Pang and X. S. Zhao, *New J. Chem.*, 2014, **38**, 616–623.
17 K. Tang, L. J. Fu, R. J. White, L. H. Yu, M. M. Titirici, M. Antonietti and J. Maier, *Adv. Energy Mater.*, 2012, **2**, 873–877.
18 Z. Q. Zhu, F. Y. Cheng and J. Chen, *J. Mater. Chem. A*, 2013, **1**, 9484–9490.
19 L. Zhao, Y. S. Hu, H. Li, Z. Wang and L. Chen, *Adv. Mater.*, 2011, **23**, 1385–1388.
20 Z. Yang, G. Du, Q. Meng, Z. Guo, X. Yu, Z. Chen, T. Guo and R. Zeng, *J. Mater. Chem.*, 2012, **22**, 5848–5854.
21 S.-J. Park, H. Kim, Y.-J. Kim and H. Lee, *Electrochim. Acta*, 2011, **56**, 5355–5362.
22 S.-J. Park, Y.-J. Kim and H. Lee, *J. Power Sources*, 2011, **196**, 5133–5137.
23 W. Wang, Q. Sa, J. Chen, Y. Wang, H. Jung and Y. Yin, *ACS Appl. Mater. Interfaces*, 2013, **5**, 6478–6483.
24 F.-F. Cao, X.-L. Wu, S. Xin, Y.-G. Guo and L.-J. Wan, *J. Phys. Chem. C*, 2010, **114**, 10308–10313.
25 N. D. Petkovich, S. G. Rudisill, B. E. Wilson, A. Mukherjee and A. Stein, *Inorg. Chem.*, 2014, **53**, 1100–1112.
26 B. Wang, H. Xin, X. Li, J. Cheng, G. Yang and F. Nie, *Sci. Rep.*, 2014, **4**, 37291–7.
27 X. Jiang, T. Herricks and Y. Xia, *Adv. Mater.*, 2003, **15**, 1205–1209.
28 J. Zhang, X. H. Liu, S. R. Wang, S. H. Wu, B. Q. Cao and S. H. Zheng, *Powder Technol.*, 2012, **217**, 585–590.
29 K. Huang, Y. Li and Y. Xing, *J. Mater. Res.*, 2013, **28**, 454–460.
30 L. Fu, H. Liu, H. Zhang, C. Li, T. Zhang, Y. Wu and H. Wu, *J. Power Sources*, 2006, **159**, 219–222.
31 Y. S. Hu, L. Kienle, Y. G. Guo and J. Maier, *Adv. Mater.*, 2006, **18**, 1421–1426.
32 J. Xu, C. Jia, B. Cao and W. Zhang, *Electrochim. Acta*, 2007, **52**, 8044–8047.
33 A. R. Armstrong, G. Armstrong, J. Canales, R. García and P. G. Bruce, *Adv. Mater.*, 2005, **17**, 862–865.
34 Z. Hong, M. Wei, T. Lan and G. Cao, *Nano Energy*, 2012, **1**, 466–471.
35 L. Zeng, C. Zheng, L. Xia, Y. Wang and M. Wei, *J. Mater. Chem. A*, 2013, **1**, 4293–4299.
36 V. G. Pol, S.-H. Kang, J. M. Calderon-Moreno, C. S. Johnson and M. M. Thackeray, *J. Power Sources*, 2010, **195**, 5039–5043.
37 A. K. Rai, L. T. Anh, J. Gim, V. Mathew, J. Kang, B. J. Paul, J. Song and J. Kim, *Electrochim. Acta*, 2013, **90**, 112–118.
38 Z. Yang, D. Choi, S. Kerisit, K. M. Rosso, D. Wang, J. Zhang, G. Graff and J. Liu, *J. Power Sources*, 2009, **192**, 588–598.
39 M. Reddy, G. Subba Rao and B. Chowdari, *Chem. Rev.*, 2013, **113**, 5364–5457.
40 L. Liu, Q. Fan, C. Sun, X. Gu, H. Li, F. Gao, Y. Chen and L. Dong, *J. Power Sources*, 2012, **221**, 141–148.

